Sensorless Control of the Synchronous Reluctance Machine

A. Kilthau, J. M. Pacas
Institute of Power Electronics and Electrical Drives
University of Siegen / FB12, LEA
Hölderlinstraße 3
57068 Siegen (Germany)

Abstract—The paper deals with the control of the synchronous reluctance machine without position sensor. A method for the computation of the transformation angle out of terminal voltages and currents is presented. The injection of test signals allows operation at zero speed. Fundamental for this control scheme is the exact modelling of the machine, where especially the saturable inductances are of central interest. The accuracy of the angle estimation method over the whole operating range including field-weakening is discussed in detail. The implementation of the angle estimation method in a rotor-oriented control scheme and practical results are demonstrated.

I. Introduction

It is well known that the synchronous reluctance machine is an alternative to permanent magnet synchronous and induction machines. Compared with permanent magnet synchronous machines it has lower costs and can function at very high speed because of the easier field weakening capability and the rugged rotor. If compared to asynchronous machines it has theoretically no rotor losses and a comparable torque density depending on the design of the machine.

On the other hand, the complexity of the dynamic equations of the synchronous reluctance machine is increased due to the different magnetic characteristics in the axis d and q. As a result, the control of synchronous reluctance machines faces some special problems different to other AC machines.

The vector control of the synchronous reluctance machine leads to structures where the saturable inductances L_d and L_q are of central interest. Particularly in sensorless control schemes the model of the machine and its parameters should describe the system as good as possible. In the case of the synchronous reluctance machine the obvious sensorless control method is to evaluate the magnetic unbalance of the rotor. The presented method is confirmed by experiment. For the experimental work a commercial available machine was used.

II. Mathematical Model

The synchronous reluctance machine can be described by the following well known set of equations in the d-q-reference frame:

$$u_d = R_s i_d + \frac{d\psi_d}{dt} - \omega\psi_q \;,\; \psi_d = L_d i_d$$
$$u_q = R_s i_q + \frac{d\psi_q}{dt} + \omega\psi_d \;,\; \psi_q = L_q i_q \qquad (1)$$

$$M_i = \frac{3}{2} p \left(L_d - L_q\right) i_d i_q \qquad (2)$$

$$J\frac{d\omega_{mech}}{dt} = M_i - M_L \;,\; \omega_{mech} = \frac{\omega}{p} \qquad (3)$$

The iron saturation can be easily considered by assuming the inductances dependent on the currents. Since the cross coupling is taken into account each inductance is dependent both on i_d and i_q:

$$\psi_d = L_d(i_d, i_q)\cdot i_d$$
$$\psi_q = L_q(i_d, i_q)\cdot i_q \qquad (4)$$

Hence by using the derivation rules (1) becomes:

$$u_d = R_s i_d + L_{dt}\frac{di_d}{dt} + i_d\left(\frac{\partial L_d}{\partial i_q}\frac{di_q}{dt}\right) - \omega L_q i_q$$
$$u_q = R_s i_q + L_{qt}\frac{di_q}{dt} + i_q\left(\frac{\partial L_q}{\partial i_d}\frac{di_d}{dt}\right) + \omega L_d i_d \qquad (5)$$

with:

$$L_{dt} = L_d + i_d\frac{\partial L_d}{\partial i_d}$$
$$L_{qt} = L_q + i_q\frac{\partial L_q}{\partial i_q} \qquad (6)$$

Equation (5) and (6) can be interpreted as follows:
The inductances L_d and L_q determine in steady-state operation the mean value of the induced voltage and the torque. The transient inductances L_{dt} and L_{qt} affect the changes of current and flux and an additional term dependent on the grade of cross coupling creates a transient disturbance voltage.

Fig. 1 shows the measured machine parameters. The inductances are the result of a current decay test [1].

III. Estimation Of The Transformation Angle

Aim of the presented sensorless control scheme is to calculate the transformation angle out of the terminal voltages and currents. The basic requirement for this kind of doing is an accurate machine model, provided with the measurements in [1]. The estimation of the rotor position angle γ will be carried out by using the developed nonlinear and deterministic model and a test signal in the lower speed range.

Equation (5) can be expressed in terms of the measured currents and voltages (U, V):

$$a_d \cdot \sin(\gamma_e) + b_d \cdot \cos(\gamma_e) = 0$$
$$a_q \cdot \sin(\gamma_e) + b_q \cdot \cos(\gamma_e) = 0 \qquad (7)$$

where a_d, a_q, b_d and b_q are the coefficients according to (8) and γ_e is the rotor position angle to be estimated.

The currents in the terms $i_d \cdot \partial L_d/\partial i_q$ and $i_q \cdot \partial L_q/\partial i_d$ are not converted to UVW-coordinates because otherwise the equations cannot be solved for γ_e. For the machine parameters L_d, L_q, L_{dt}, L_{qt} the respective values calculated with the currents i_d, i_q of the previous control interval are used.

After the calculation of the coefficients a_d, b_d, a_q and b_q out of the model parameters of the previous control interval and the voltages u_U, u_V and currents i_U, i_V of the actual control interval (7) can be solved for γ_e:

$$\gamma_{e1} = \begin{cases} -atan\left(\dfrac{b_{d,q}}{a_{d,q}}\right) & \text{for} \quad a_{d,q} \geq 0 \\ -atan\left(\dfrac{b_{d,q}}{a_{d,q}}\right) + \pi & \text{for} \quad a_{d,q} < 0 \end{cases} \qquad (9)$$
$$\gamma_{e2} = \gamma_{e1} + \pi$$

Equation (7) has two possible solutions γ_{e1} and γ_{e2}. In the case of the synchronous reluctance machine both solutions are valid because the synchronous reluctance machine has no rotor winding or permanent magnets. However it must be ensured that the estimation algorithm uses only one of these two solutions. A displacement of γ_e by 180 degrees would cause a sign reversal of voltages and currents.

The meaning of the coefficients a_d, a_q, b_d and b_q can be illustrated by applying the transformation rules once again to (8). This leads to the more transparent relationships

$$a_d = -c_d \cdot \cos(\gamma_e) \qquad a_q = c_q \cdot \cos(\gamma_e)$$
$$b_d = c_d \cdot \sin(\gamma_e) \qquad b_q = -c_q \cdot \sin(\gamma_e) \qquad (10)$$

with

$$c_d = \omega\left(L_d - L_q\right) i_d - \left(L_{dt} - L_{qt}\right)\frac{di_q}{dt} + \left(i_d \frac{\partial L_d}{\partial i_q} + i_q \frac{\partial L_q}{\partial i_d}\right)\cdot\frac{di_d}{dt}$$
$$c_q = \omega\left(L_d - L_q\right) i_q + \left(L_{dt} - L_{qt}\right)\frac{di_d}{dt} + \left(i_d \frac{\partial L_d}{\partial i_q} + i_q \frac{\partial L_q}{\partial i_d}\right)\cdot\frac{di_q}{dt} \qquad (11)$$

For a good quality of angle estimation the coefficients c_d and c_q must be significant greater than zero. The first term in c_d and c_q represents the induced EMF and can be used for angle estimation at higher speed. At standstill the angle can be estimated using the second term. In this case di/dt can be increased by injecting a superimposed alternating voltage. The third term is caused by cross saturation effects. It will be shown that the consideration of this term increases the accuracy of the estimation.

Fig. 2 shows the charts of c_d and c_q when there is no superimposed voltage. These considerations are necessary to select the regions where the angle is calculated out of a_d, b_d or out of a_q, b_q. It can be seen that at no-load the angle must be estimated using a_d and b_d because c_q is zero. At high load and high speed the estimation of γ_e using a_q and b_q is expected to give the better results because c_q is greater than c_d.

A. Angle Estimation at Slow Speed

At zero speed both c_d and c_q in Fig. 2 become zero. According to (11) c_d can be increased at $\omega=0$ when increasing di_q/dt and c_q can be increased when increasing di_d/dt. This can be achieved by injecting a rectangular voltage $\pm\Delta u$ in the required axis. The period of the superimposed voltage is selected to be 600µs. The currents are measured at the beginning of each control interval of 150µs, so di/dt is calculated out of the difference between current measurements of a 300µs-interval. The amplitude of the superimposed voltage is set to $\Delta u = \pm 200V$.

Using (5) di_d/dt and di_q/dt can be expressed as functions of Δu. Fig. 3 shows the resulting characteristics c_d and c_q with a superimposed voltage Δu in the d- or q-axis. Because L_{dt} is greater than L_{qt} the magnitude of di_d/dt and c_q is smaller than the magnitude of di_q/dt and c_d. Also c_q becomes zero at certain values $i_q<0$. Therefore the angle should be estimated using a_d, b_d with injection of Δu in the q-axis. An additional problem is the magnitude of c_d at $i_q=0$. The reason is that the difference L_{dt}-L_{qt} in (11) at the currents $i_d=10A$ and $i_q=0$ is nearly zero. The entire dependence of c_d on i_d and i_q at standstill is shown in Fig. 4. Because L_{dt} increases as i_d decreases the current i_d must be decreased at small values of i_q in order to get a value of c_d significantly greater than zero, see Fig. 5.

B. Estimation Strategy

The aim of the following considerations is to obtain a magnitude of c_d or c_q as high as possible in each operation point. For this purpose the n-i_q-plane is divided into 4 sections, see Fig. 6. The resulting magnitudes of c_d and c_q are shown in Fig. 7.

$$a_d = \frac{1}{\sqrt{3}}\cdot\left[\left(R_s + \sqrt{3}\,\omega\left(L_q - L_{dt}\right) - \omega i_d \frac{\partial L_d}{\partial i_q}\right)\cdot i_U + 2\left(R_s - \omega i_d \frac{\partial L_d}{\partial i_q}\right)\cdot i_V + \left(L_{dt} - \sqrt{3} i_d \frac{\partial L_d}{\partial i_q}\right)\cdot\frac{di_U}{dt} + 2L_{dt}\cdot\frac{di_V}{dt} - u_U - 2u_V\right]$$
$$b_d = \frac{1}{\sqrt{3}}\cdot\left[\left(\sqrt{3}R_s - \omega\left(L_q - L_{dt}\right) - \sqrt{3}\,\omega i_d \frac{\partial L_d}{\partial i_q}\right)\cdot i_U - 2\omega\left(L_q - L_{dt}\right) i_V + \left(\sqrt{3}L_{dt} + i_d \frac{\partial L_d}{\partial i_q}\right)\cdot\frac{di_U}{dt} + 2i_d \frac{\partial L_d}{\partial i_q}\cdot\frac{di_V}{dt} - \sqrt{3}u_U\right]$$
$$a_q = \frac{-1}{\sqrt{3}}\cdot\left[\left(\sqrt{3}R_s - \omega\left(L_d - L_{qt}\right) + \sqrt{3}\,\omega i_q \frac{\partial L_q}{\partial i_d}\right)\cdot i_U - 2\omega\left(L_d - L_{qt}\right) i_V + \left(\sqrt{3}L_{qt} - i_q \frac{\partial L_q}{\partial i_d}\right)\cdot\frac{di_U}{dt} - 2i_q \frac{\partial L_q}{\partial i_d}\cdot\frac{di_V}{dt} - \sqrt{3}u_U\right] \qquad (8)$$
$$b_q = \frac{1}{\sqrt{3}}\cdot\left[\left(R_s + \sqrt{3}\,\omega\left(L_d - L_{qt}\right) + \omega i_q \frac{\partial L_q}{\partial i_d}\right)\cdot i_U + 2\left(R_s + \omega i_q \frac{\partial L_q}{\partial i_d}\right)\cdot i_V + \left(L_{qt} + \sqrt{3} i_q \frac{\partial L_q}{\partial i_d}\right)\cdot\frac{di_U}{dt} + 2L_{qt}\cdot\frac{di_V}{dt} - u_U - 2u_V\right]$$

1) In the range of $-1000\text{min}^{-1}<n<1000\text{min}^{-1}$ a rectangular voltage of ±200V is injected in the q-axis. At speed higher than 1000min^{-1} the superimposed voltage would reach the voltage limit of the inverter or the absolute value of c_d at $\Delta u_q=+200V$ would become too small (see Fig. 7). The selected reduction strategy of i_d in this region shows Fig. 5.

2)-4) For speed above 1000min^{-1} the method which results in the highest amplitude of c_d or c_q is selected.

In this way the magnitudes of c_d and c_q are never equal to zero, see Fig. 7. Additionally to the considerations above it must be selected among the two possible solutions γ_{e1} and γ_{e2} in (9):

$$\gamma_e=\begin{cases}\gamma_{e1} & \text{for } c_d<0,\ -c_q<0\\ \gamma_{e2} & \text{for } c_d>0,\ -c_q>0\end{cases} \tag{12}$$

C. *Speed and position observer*

Using the described method the rotor angle can be estimated with sufficient accuracy. Still there are problems at dynamic variations of the currents. In this case the stationary characteristics of c_d and c_q shown in Fig. 7 are not valid because of the term di/dt in (11), and therefore some estimated values γ_e become incorrect at small values of c_d or c_q. It is also impossible to get a speed value with sufficient accuracy by derivation of the estimated angle due to the noise in this signal. The described problems can be solved by using an observer for the mechanical subsystem of the machine.

The general form of a state-space model is:

$$\begin{aligned}\frac{d\mathbf{x}(t)}{dt}&=\mathbf{A}\cdot\mathbf{x}(t)+\mathbf{B}\cdot\mathbf{u}(t)+\mathbf{E}\cdot\mathbf{z}(t)\\ \mathbf{y}(t)&=\mathbf{C}\cdot\mathbf{x}(t)+\mathbf{D}\cdot\mathbf{u}(t)\end{aligned} \tag{13}$$

By applying the equations of the mechanical subsystem of the machine to (13) the state-space model becomes:

$$\begin{aligned}\frac{d}{dt}\begin{pmatrix}\omega(t)\\ \gamma(t)\end{pmatrix}&=\begin{pmatrix}0 & 0\\ 1 & 0\end{pmatrix}\cdot\begin{pmatrix}\omega(t)\\ \gamma(t)\end{pmatrix}+\begin{pmatrix}\frac{p}{J}\\ 0\end{pmatrix}\cdot M_i(t)+\begin{pmatrix}-\frac{p}{J}\\ 0\end{pmatrix}\cdot M_L(t)\\ \gamma(t)&=\begin{pmatrix}0 & 1\end{pmatrix}\cdot\begin{pmatrix}\omega(t)\\ \gamma(t)\end{pmatrix}+0\cdot M_i(t)\end{aligned} \tag{14}$$

The disturbance variable M_L is unknown. Still it is possible to consider the disturbance variable if the time characteristic of the disturbance is basically known. Here the load torque is assumed to be constant. Therefore the disturbance model is:

$$\frac{d}{dt}M_L=0 \tag{15}$$

The observer structure can be derived out of (14) and (15) in a formal way (see Fig. 8). The dynamic of the observer is given by the feedback coefficients l_1 and l_2.

In the case of $M_L\neq\hat{M}_{L0}$ the difference between reality and model is compensated by the feedback variable r_1 in Fig. 8. As a consequence there is a stationary error in $\hat{\gamma}$ and $\hat{\omega}$ dependent on M_L, l_1 and l_2. The stationary error in $\hat{\omega}$ can be eliminated by using the signal $d\hat{\gamma}/dt$ as speed variable, but then the noise of the estimated angle γ_e deteriorates the quality of the estimated speed.

These disadvantages are eliminated by using the observer structure in Fig. 9. With the integrator in the feedback loop the stationary error of $\hat{\gamma}$ and $\hat{\omega}$ becomes zero.

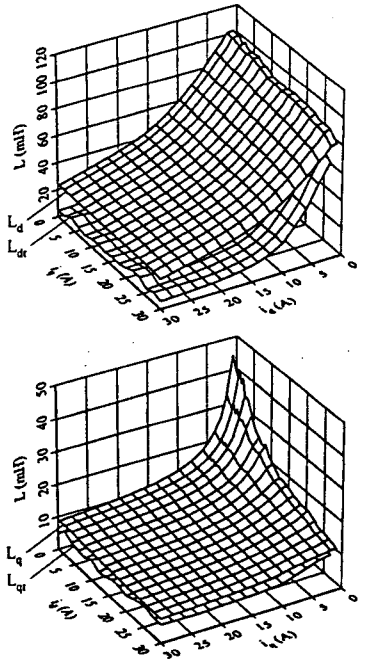

Fig. 1: Stationary inductances L_d, L_q and transient inductances L_{dt}, L_{qt} measured with the current decay test.

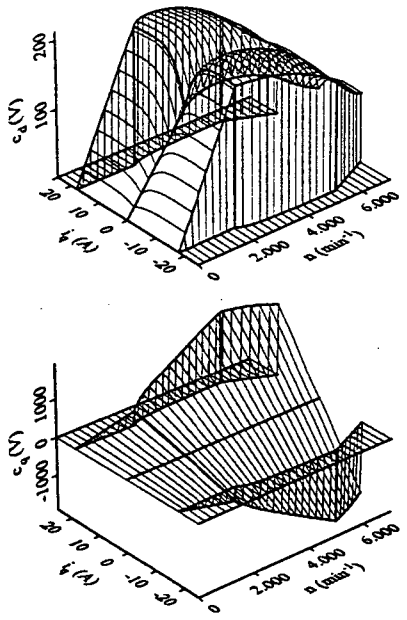

Fig. 2. Magnitude of c_d and c_q without superimposed voltage.

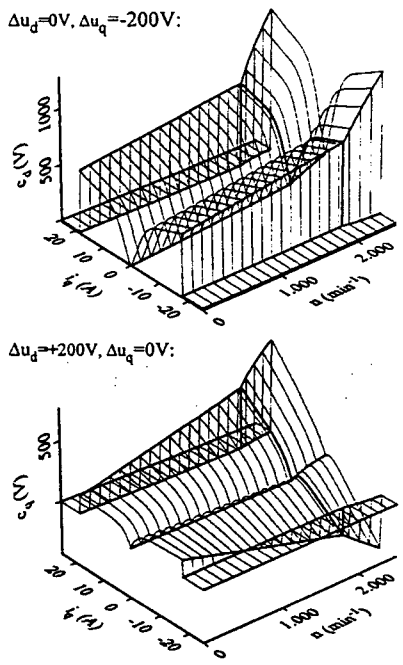

Fig. 3. Magnitude of c_d and c_q with superimposed voltage in base speed range.

IV. Experimental Results

The control scheme has been realized in the laboratory. The simplified control scheme is shown in Fig. 10, see also [2]. The DC link voltage is controlled to a fix value of 670V. The inverter uses a space vector PWM, the switching frequency is 3,3kHz and the sample time is 150µs. The inductance characteristics are implemented by using polynomials with a order of 6 ($L_d(i_d)$) and 9 ($L_q(i_q)$) and with a linear dependence $L_d(i_q)$ and $L_q(i_d)$.

First the machine is operated with an angular sensor for the control. The measured angle γ and the estimated angle γ_e are compared directly in order to verify the estimation algorithm. The average difference $\gamma - \gamma_e$ at n=20min^{-1} and

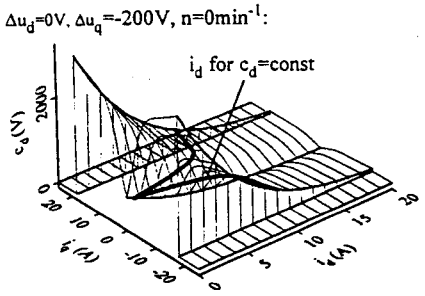

Fig. 4. Magnitude of c_d as a function of i_d, i_q at standstill and with superimposed voltage.

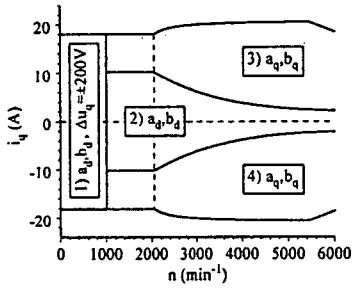

Fig. 6. Regions where the angle γ is calculated out of a_d, b_d or a_q, b_q.

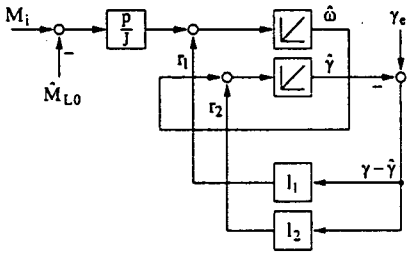

Fig. 8. Formal structure of the observer.

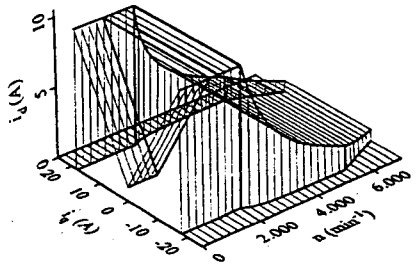

Fig. 5. Complete i_d-characteristic with reduction of i_d when applying an additional voltage at slow speed.

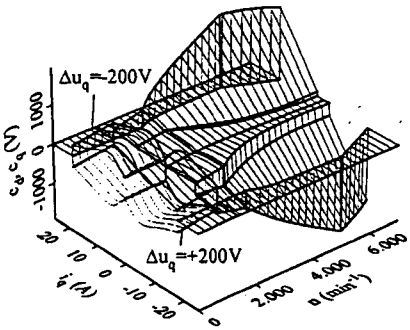

Fig. 7. Resulting magnitudes of c_d and c_q.

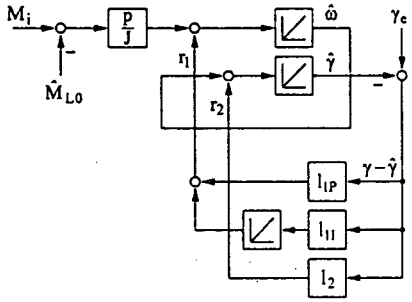

Fig. 9. Enhanced structure of the observer with PI feedback.

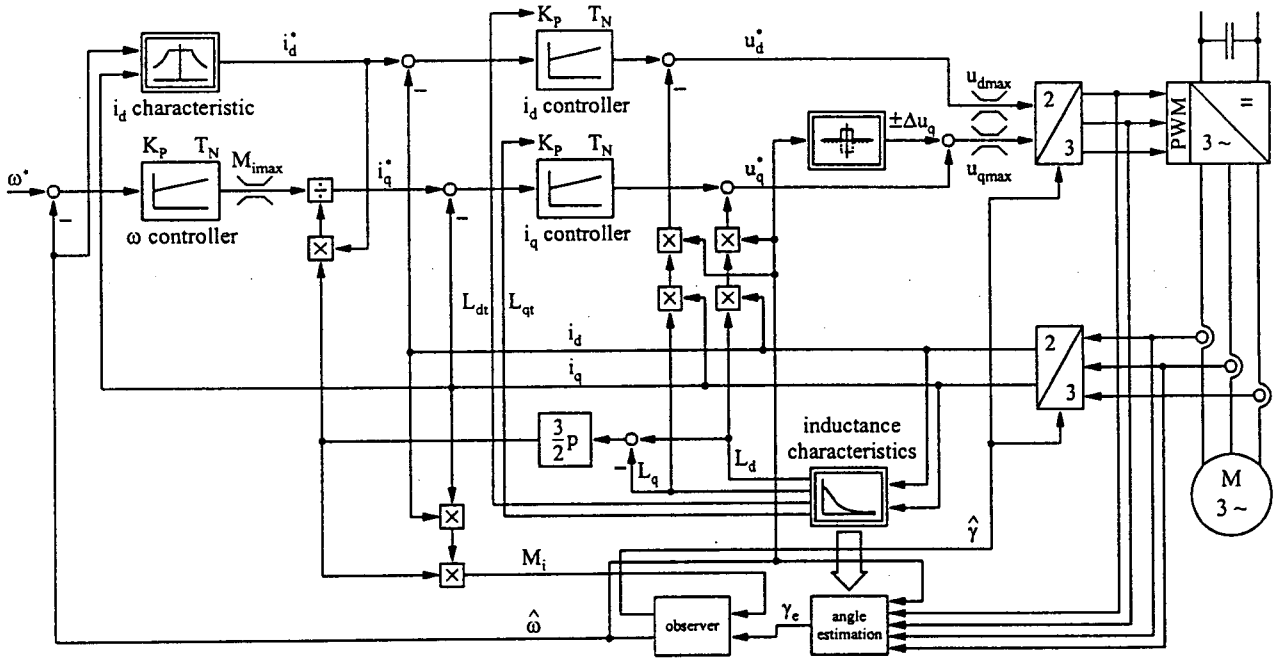

Fig. 10. Control scheme of the synchronous reluctance machine.

n=2000min^{-1} shows Fig. 11. Normally the error is less than 2 degrees, only at i_q=0 and with superimposed voltage (n=20min^{-1}) the error increases. The dotted curves in Fig. 11 show the error when the di/dt- or the cross saturation-term in (8) is neglected. Thus it is proved that consideration of the cross saturation increases the estimation accuracy.

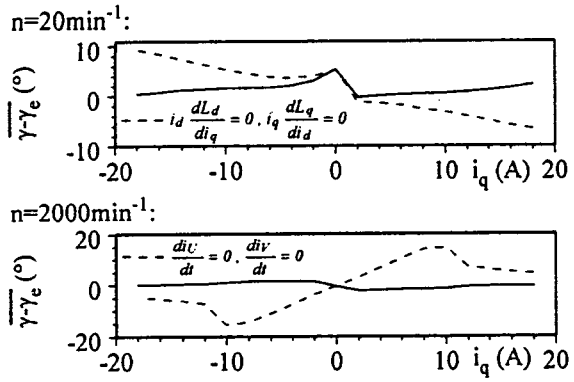

Fig. 11. Average difference between measured and estimated angle.

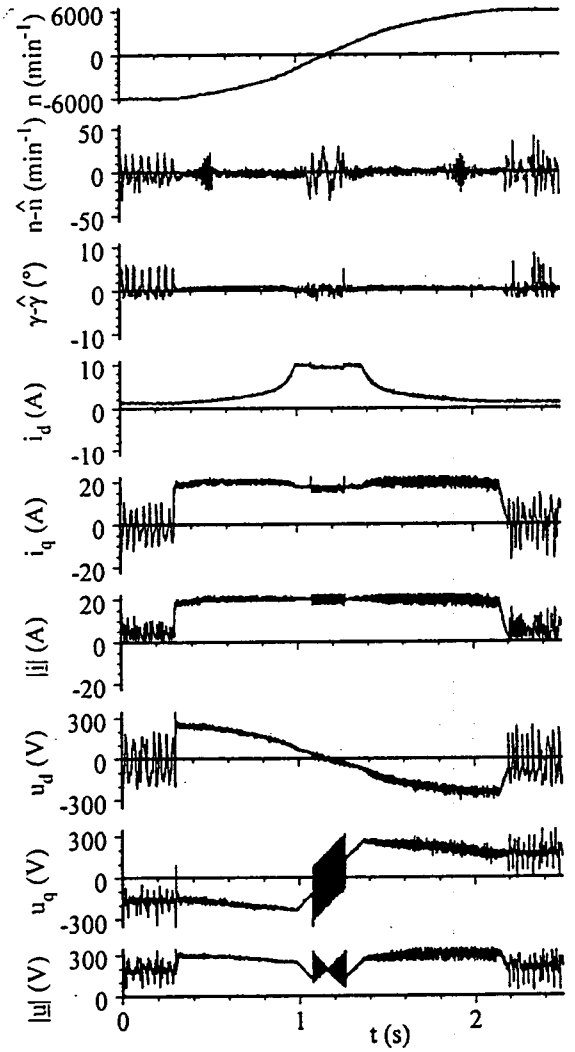

Fig. 12. Measured control variables during speed reversal with additional load inertia of 11·10^{-3} kgm^2.

In the next step the machine is controlled according to Fig. 10 using the observed variables $\hat{\gamma}$ and $\hat{\omega}$. Fig. 12 shows a speed reversal from –6000 to +6000min^{-1} and the errors of the observed speed and position.

V. Conclusion

This paper presents a sensorless control scheme for the synchronous reluctance machine. The calculation method uses one measured value of the currents per control cycle, so additional measurements are not necessary. Using the presented model of the machine, the transformation angle can be estimated out of the terminal voltages and currents over the whole speed and load range by means of a non-linear deterministic model with high accuracy. This investigation is a basic work regarding the use of the synchronous reluctance machine in speed-controlled low-cost electrical drives.

VI. Machine Data

ABB servomotors, type 2E5.7

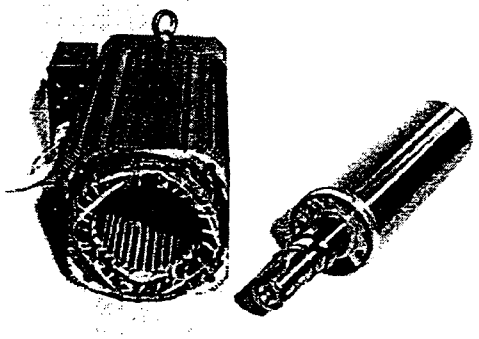

rated torque	M_r=27 Nm
rated current	I_r=14,6 A
number of poles	p=4
rotor inertia	J=7,041·10^{-3} kgm^2
stator resistance	R_S=0,34 Ω

References

[1] Kilthau, A.; Pacas, J. M.: Measurement of the Parameters of the Synchronous Reluctance Machine including Cross Saturation. EPE Graz, Aug. 2001.

[2] Kilthau, A.; Pacas, J. M.: Control of Synchronous Reluctance Machines. PCIM Nürnberg, June 2001.

[3] Vagati, A.; Pastorelli, M.; Scapino, F.; Franceschini, G.: Impact of cross saturation in synchronous reluctance motors of the transverse-laminated type. IEEE Transactions on Industry Applications, Vol.36, No.4; July/ Aug. 2000, S. 1039-1046

[4] Kang, S-J; Kim, J.-M.; Sul, S.-K.: Position sensorless control of synchronous reluctance motor using high frequency current injection. IEEE Transactions on Energy Conversion, Vol.14, Dec.1999, S.1271-1275

[5] Jovanovic, M.G.; Betz, R. E.; Platt, D.: Sensorless vector controller for a synchronous reluctance motor. IEEE Transactions on Industry Applications, Vol. 34, No. 2, March/April 1998, S. 346-353.

[6] Chomat, M.; McCulloch, M. D.: Simulation and control of saturated synchronous reluctance machine. EPE Trondheim 1997, S. 3564-3569.

[7] Franceschini, G.; Fratta, A.; Petrache, C.; Vagati, A.: Control of high performance synchronous reluctance drives. Intelligent Motion, June 1994, S. 117-126.

[8] Sack, L.: Attributes of servo drive systems with reluctance motors. EPE Grenoble 1987, S. 923-928.